Image Segmentation Errors Correction by Mesh Segmentation and Deformation

Achia Kronman and Leo Joskowicz

School of Eng. and Computer Science, The Hebrew Univ. of Jerusalem, Israel
achiak@cs.huji.ac.il

Abstract. Volumetric image segmentation methods often produce delineations of anatomical structures and pathologies that require user modifications. We present a new method for the correction of segmentation errors. Given an initial geometrical mesh, our method semi automatically identifies the mesh vertices in erroneous regions with min-cut segmentation. It then deforms the mesh by correcting its vertex coordinates with Laplace deformation based on local geometrical properties. The key advantages of our method are that: 1) it supports fast user interaction on a single surface rendered 2D view; 2) its parameters values are fixed to the same value for all cases; 3) it is independent of the initial segmentation method, and; 4) it is applicable to a variety of anatomical structures and pathologies. Experimental evaluation on 44 initial segmentations of kidney and kidney vessels from CT scans show an improvement of 83% and 75% in the average surface distance and the volume overlap error between the initial and the corrected segmentations with respect to the ground-truth.

1 Introduction

Patient-specific models of anatomical structures and pathologies generated from volumetric medical images play an increasingly central role in many clinical applications, including, among many others: 1) accurate volumetric radiological measurements of healthy and diseased structures for diagnosis, treatment determination, and follow-up assessment; 2) treatment planning in radiation therapy; 3) preoperative surgery planning and intra-operative navigation, and; 4) surgery rehearsal and training by simulation.

Medical image segmentation is the key step of patient-specific modeling. Numerous segmentation methods have been developed in the past. However, most are not used in clinical practice because they lack robustness, require extensive physician input, and/or require technical assistance. Indeed, segmentation is a very challenging task mostly due to: 1) wide imaging variability resulting from different imaging modalities, scanning protocols, and scanners parameters; 2) large intra- and inter- patient anatomical variability, and; 3) intensity values overlap between structures tissues and their proximity.

As a result, medical image segmentations often contain errors and require user modifications. Segmentation correction can be a tedious and time-consuming

K. Mori et al. (Eds.): MICCAI 2013, Part II, LNCS 8150, pp. 206–213, 2013.

task: the user is required to examine the image slices with the delineation of the structures superimposed on them and to correct them where needed. When the segmentation results of a particular method frequently require corrections, it will not be used in clinical practice. Hence an automatic or semi-automatic method for segmentation correction with fast and intuitive user interaction is essential for its clinical acceptance.

Several semi-automatic methods for segmentation correction have been proposed in the past. Boykov et al. [1] describe an interactive algorithm for the correction of segmentation errors. Their method corrects the segmentation with min-cut energy minimization, using user-provided seeds for the corrections, where the graph weights are being changed in each iteration according to the new seeds. Grady et al. [2] use, in addition to user-provided seeds, the initial segmentation as a soft prior for the correct segmentation. However, their method requires precise parameter tuning to balance two opposite factors – the initial segmentation prior and the user provided-seeds. In addition, it requires tuning the locality of the seeds influence, which may be different for each case. Heckel et al. [3] use a live-wire based extrapolation of a user-provided 2D contour. In this method, the processing is performed on each 2D slice separately by copying the corrected contours of the adjacent slices and then adjusting them. This method requires specific parameter tuning for the copy stopping criteria that may not be suitable for complex structures such as vessel trees with bifurcations.

In this paper we present a new geometrical method for the correction of segmentation errors. Given an initial segmentation, represented as a geometrical mesh, we apply a three-step algorithm. The first step is the segmentation of the mesh vertices to identify and correct the erroneous regions with curvature-based min-cut segmentation. The second step is the modification of the erroneous vertices to their correct coordinates with Laplace deformation, using the mesh segmentation as boundary conditions. The third step is the identification of the actual structure of interest and its final re-meshing.

Our method has the following advantages: 1) it is independent of the initial segmentation method; 2) it supports an easy and intuitive 2D user interaction, both in the image-space and on a single 2D surface-rendered view on the screen. 3) its internal parameters values are fixed to the same value for all cases; 4) it is applicable to a variety of anatomies and pathologies, including complex structures such as vessels trees, and; 5) its computational complexity depends only on the size of the initial segmentation and is independent of the image size. Our experimental evaluation on 44 initial segmentations of kidney and kidney vessels from clinical CT scans shows a mean improvement of 83% and 75% in the average surface distance and the volume overlap error between the initial and the corrected segmentations with respect to the ground-truth.

2 Method

Our method focuses on correcting segmentation errors of an initial segmentation S that has the same topology as the ground truth GT, but may be different with

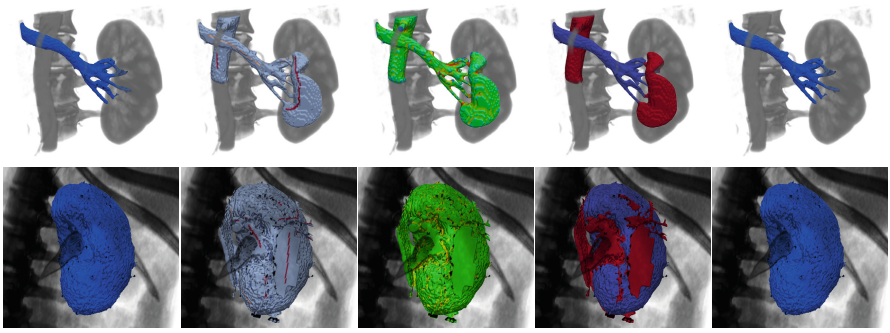

(a) (b) (c) (d) (e)

Fig. 1. Illustration of the algorithm steps: meshes of kidney vessels (top) and kidney contour (bottom) superimposed on volume-rendered kidney images. (a) initial segmentation with leaks; (b) user defined scribbles (red and light brown); (c) minimum principal curvature – warm colors indicate lower curvature values; (d) min-cut mesh segmentation to correct (blue) and leak (red) regions; (e) final meshes after correction.

respect to the ground truth geometry. i.e. with respect to its surface coordinates location. This is justified by the empirical observation that the vast majority of segmentation errors belong to this class.

We distinguish between two types of segmentation geometrical errors: *outer leaks* and *inner leaks*. Segmentation outer leaks occur when the segmentation volume expands outside the target volume into neighboring structures, mostly due to low contrast between the neighboring structures. Segmentation inner leaks occur when the segmentation stops in the interior of the target volume, mostly due to the existence of strong gradients in the interior of the target structure. Our segmentation errors correction method deals with both types of errors.

The algorithm consists of three steps: 1) segmentation of the correct vs. incorrect regions of the segmentation surface by geometry-based min-cut mesh segmentation; 2) deformation of the incorrect segmentation regions to their correct location by Laplace-Poisson deformation based on local geometrical criteria, and; 3) structure component identification and remeshing. We describe next the algorithm inputs and these three steps in detail.

2.1 Algorithm Inputs

The two inputs to the algorithm are: 1) an initial mesh $S = \{V, E\}$ with vertices $V = \{v_i\}$ and edges $E = \{e_i\}$. The mesh S may be obtained with any segmentation method – e.g., with the marching-cubes algorithm and binary image classification (Fig. 1a), and; 2) user-defined "scribbles" on the mesh surface to indicate the parts that do/do not belong to the structure of interest. We use the scribble information as seeds to classify the mesh regions and to correct the segmentation leaks (Fig. 1b).

We distinguish between three types of scribbles in V: 1) vertices that the user marks as lying on the true surface of the target structure, $Seed_{correct}$; 2) vertices that the user marks as segmentation outer leaks, $Seed_{out}$, and; 3) vertices that the user mark as segmentation inner leaks, $Seed_{in}$.

The user defines these scribbles by interaction on a single 2D surface rendering of S. Note that this kind of interaction is faster and far more intuitive then defining them on numerous 2D contours overlaid on the CT scan as it is customary in existing methods. The scribbles are projected onto the 3D model surface. Note that our method also supports interaction on the CT slices if they are preferred by the user.

2.2 Segmentation Errors Detection by Min-cut Mesh Segmentation

This step assigns a label l to each vertex $v_i \in V$, such that $l(v_i) \in \{non\ leak,$ $outer\ leak, inner\ leak\}$, where *non leak* label the vertices that lie on the true surface of the target structure and *outer leak* and *inner leak* label the leak vertices, respectively.

The segmentation is based on the observation that the interface between the true surface and the outer leaks is usually concave, while the interface between the true surface and the inner leaks is usually convex. We model the degree of concavity and convexity of a mesh vertex with the minimal and maximal principal curvature of the mesh vertex as follows.

Let κ_i^{min} and κ_i^{max} be the minimal and maximal principal curvature of vertex v_i as defined in [4]. Lower values of κ_i^{min} indicate vertices that may be part of the interface between the correct and the outer leaks regions; higher values of κ_i^{max} indicate vertices that may be part of the interface between the correct and the inner leaks regions. Fig. 1c shows an example of displaying the minimum principal curvature on top of the input mesh.

Since the exact values of the interface curvatures are unknown and may be different for each case, a simple curvature thresholding is not an appropriate solution. Instead, we compute the mesh segmentation by minimizing energy functions that incorporate both the vertex curvature and the location of the user seeds from the scribbles. We define two energy functions, one for the segmentation of the outer leaks and one for the segmentation of the inner leaks. We define our first energy function $E_{out}(s)$ as follows:

$$E_{out}(S) = \sum_{v_i \in V} f_{out}(v_i) + \sum_{v_i \in V} \sum_{u_i \in N(v_i)} g_{\kappa^{min}}(u_i, v_i) \tag{1}$$

where $N(v_i)$ are the neighbor vertices of v_i in S. The first term is:

$$f_{out}(v_i) = \begin{cases} \infty & v_i \in Seed_{out} \text{ and } l^{out}(v_i) = outer\ leaks \\ 0 & v_i \in Seed_{out} \text{ and } l^{out}(v_i) \neq outer\ leaks \\ 0 & v_i \in Seed_{correct} \text{ and } l^{out}(v_i) = outer\ leaks \\ \infty & v_i \in Seed_{correct} \text{ and } l^{out}(v_i) \neq outer\ leaks \\ 0.5 & \text{otherwise} \end{cases} \tag{2}$$

where $l^{out}(v_i)$ labels v_i as *outer leak* or one of the other two labels. This term guarantees that the seeds will always have the correct label.
The second term is:

$$g_{\kappa^{min}}(u_i, v_i) = \begin{cases} 1/e^{-a(\kappa_{u_i}^{min} + \kappa_{v_i}^{min})/\sigma^2} & u_i \text{ and } v_i \text{ has different labels} \\ 0 & u_i \text{ and } v_i \text{ has the same label} \end{cases} \quad (3)$$

for positive constant parameters a and σ. This term guarantees that edges with lower vertex curvature will have lower cost.

Similarly, we define a second energy function, $E_{in}(s)$, to account for the separation of the inner leaks from the other labels. We use the same formulation as we used for $E_{out}(s)$ in Equation (1), replacing in Equation (2) $Seed_{out}$ with $Seed_{in}$, label *outer leaks* with label *inner leaks*, and replacing in Equation (3) the minimal principal curvature κ^{min} with the maximal principal curvature κ^{max}, and the constant parameter a with the opposite of the same parameter in the first energy equation.

We then perform an independent global minimization for each energy function with the min-cut algorithm [5]. The results are the corresponding labeling $l^{out}(v_i)$ and $l^{in}(v_i)$ that minimize each of the two energy functions defined above (Fig. 1d).

Finally, we compute the final mesh labeling $l(v_i) \in \{leak,\ non\ leak\}$ by labeling each label as *leak* if it is labeled by E_{out} as *outer leak* or by E_{in} as $inner - leak$, otherwise it is labeled as *non leak*. Formally:

$$l(v_i) = \begin{cases} leak & l^{out}(v_i) = outer\ leak\ \vee\ l^{in}(v_i) = inner\ leak \\ non\ leak & else \end{cases} \quad (4)$$

2.3 Errors Correction by Laplace-Poisson Mesh Deformation

Once the classification has been performed, we compute the new coordinates of the leak vertices based on the local smoothness properties of anatomical structures. To obtain the smoothest surface, we use Laplace interpolation with Dirichlet boundary conditions, which minimizes the sum of the squared vertex gradients. The Laplace interpolation is formulated as:

$$\begin{aligned} \nabla^2(v_i) = \sum_{u_j \in N(v_i)} (v_i - u_j) = 0, \qquad \forall v_i : l(v_i) = leak \\ \text{subject to:} \qquad u_j = u_j^* \qquad \forall u_j : l(u_j) = non\ leak \end{aligned} \quad (5)$$

where $v_i = (x_i, y_i, z_i)$ are the new vertex coordinates, $\nabla^2 v_i$ is the discrete graph Laplacian operator [6], u_j are the neighbors of v_i, and u_j^* are the known coordinates of the non-leak boundary vertices. We solve the resulting sparse system of linear equations three times, one for each coordinate, by LU decomposition [7], thereby obtaining the corrected new coordinates of the leak vertices.

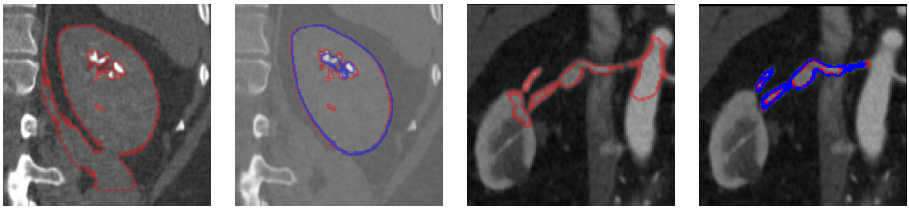

(a) (b) (c) (d)

Fig. 2. Illustration of the experimental results: (a,c) initial and (b,d) final segmentation after corrections of the kidney contour and the kidney vessels overlaid on a sample CT slice. The red contours are the initial and final segmentations after corrections; the blue contours are the ground-truth segmentations.

2.4 Structure Component Identification and Remeshing

We obtain the final image segmentation from the initial segmentation by separating it into connected components, where the computed deformed mesh serves as the separator. We then select the component that is connected to the user provided non-leak scribbles. The final mesh is obtained by applying a suitable meshing algorithm, such as the marching cubes algorithm on the resulting binary classification of the image voxels (Fig. 1e).

3 Experimental Results

We designed and conducted an experimental study to quantify our method quality, and to evaluate its scope. We retrospectively selected from the hospital database 22 CT clinical scans of two different structures, the kidney outer surface and the kidney vessels. Note that these structures have substantial differences in their shape. For the kidney contour study, we used 12 clinical CT datasets without contrast agent, of size $512 \times 512 \times 350 - 500$ voxels, $0.5 - 1.0 \times 0.5 - 1.0 \times 1.0 - 1.5\text{mm}^3$, from a Brilliance 64-row CT scanner (Phillips Healthcare, Cleveland, OH). For the kidney vessels study, we used 10 clinical arterial-phase CTA datasets of size $512 \times 512 \times 500$ voxels, $0.7 - 1.2 \times 0.7 - 1.2 \times 0.7 - 1.2\text{mm}^3$ from the same scanner. Ground-truth segmentations were obtained for both anatomies from the manual segmentation of an expert radiologist.

For each case we obtained two initial segmentations as follows. For the kidney contour segmentation, we used intensity-based min-cut segmentation with a weak shape prior generated manually with a coarse square brush inside the kidney volume. For the kidney vessel, we used the geodesic active contour level-set ITK-SNAP interactive tool [8]. The segmentation input consisted of user-defined seeds inside the target structure and parameter settings for the level-set differential equation terms. The user manually stopped the segmentation when the entire target volume was segmented. All the resulting segmentations contained segmentation leaks. We then applied our leaks correction algorithm and computed the segmentation quality improvement relative to the initial segmentation.

Table 1. Summary of evaluation metrics for the kidney and kidney vessels segmentation studies. The metrics are the Absolute Volume Difference (AVD) from the ground-truth in %, Average Symmetric Surface Distance (ASSD) in mm, the Maximal Symmetric Surface Distance (MSSD) in mm, and the Volumetric Overlap Error (VOE) in %. The first (fifth) and second (sixth) are the initial and corrected segmentation measures; the third (seventh) row is the initial corrected difference; the fourth (eighth) row is the relative improvement in %.

Structure	Type	**AVD (%)**		**ASSD (mm)**		**MSSD (mm)**		**VOE (%)**	
		mean	std	mean	std	mean	std	mean	std
Kidney contour	initial	49.2	21.3	3.1	0.7	19.7	3.3	35.1	9.2
	corrected	4.0	4.4	0.8	0.3	11.4	2.6	11.5	4.3
	improvement(Δ)	45.1	17.0	2.3	0.3	8.3	0.6	23.7	4.9
	improvement(%)	91.8	79.3	73.2	51.4	42.2	19.2	67.3	53.2
Kidney vessels	initial	334.2	188.7	5.4	2.4	24.3	8.4	72.4	13.8
	corrected	5.4	2.3	0.28	0.08	11.6	3.7	12.2	3.1
	improvement(Δ)	328.9	185.7	5.1	2.4	12.7	4.7	60.2	10.7
	improvement(%)	98.4	98.4	94.8	96.7	52.4	56.2	83.2	77.5

The mean user interaction time was 36 secs (std=16). The mean running time of the correction algorithm was 9.59 secs (std=1.57) on a 64-bit quad-core 2.80GHz processors and 6.0GB memory PC. The graph edges weights in Equation (3) were fixed to $a = 13$ and $\sigma = 1$ for all cases.

We evaluated our method with both volumetric and surface based metrics. Table 1 shows the results. Note that in all the evaluation metrics, our method significantly improves both the mean quality and its variability. The improvement for the kidney contour is 73.2% (std=10.5%) and 67.3% (std=12.3%) in the average surface distance and in the volume overlap error between the initial and the corrected segmentations with respect to the ground truth. The improvement for the kidney vessels is 94.8% (std=1.5%) and 83.2% (std=4.28%) with respect to the same metrics. Note also that these stds are the standard deviations of the segmentation quality improvement, while those in Table 1 indicate the improvement of the segmentation quality standard deviations. Fig. 2 shows representative examples.

4 Conclusion

Segmentation errors are common and pervasive in all types of segmentation methods. While their nature and prevalence varies among methods, their correction is mandatory and often requires extensive manual user interaction.

To address this issue, we have developed a new three-step method for the correction of segmentation geometrical errors. Given an initial mesh, the first step is the segmentation of the mesh vertices to identify and correct the erroneous regions based on curvature based min-cut segmentation. The second step is the deformation of the erroneous vertices to their correct coordinates with Laplace

deformation. The third step is the identification of the actual structure of interest and its final re-meshing.

The novelty of our method is in the use of user-defined scribbles on a single 2D surface rendering of the mesh surface to indicate the parts that do/do not belong to the structure of interest. This is more intuitive and faster that the commonly used method of correcting the contours on 2D slices of the original scan, as corrections in the image domain require scrolling hundreds of slices. In addition, our method is independent of the initial segmentation method and does not require internal parameters values fine-tuning. It can be applied to a variety of anatomies and pathologies, including complex structures such as vessels trees. Its computational complexity depends only on the size of the initial segmentation and is independent of the image size. Experimental evaluation on 44 initial segmentations of kidney and kidney vessels from CT scans show an average improvement of 83% and 75% in the average surface distance and the volume overlap error between the initial and the corrected segmentations with respect to the ground-truth.

Future work includes testing our method on more anatomical structures, and further expanding the proposed framework.

References

1. Boykov, Y.Y., Jolly, M.P.: Interactive graph cuts for optimal boundary & region segmentation of objects in nd images. In: Proceedings of the Eighth IEEE International Conference on Computer Vision, ICCV 2001, vol. 1, pp. 105–112. IEEE (2001)
2. Grady, L., Funka-Lea, G.: An energy minimization approach to the data driven editing of presegmented images/Volumes. In: Larsen, R., Nielsen, M., Sporring, J. (eds.) MICCAI 2006. LNCS, vol. 4191, pp. 888–895. Springer, Heidelberg (2006)
3. Heckel, F., Braunewell, S., Soza, G., Tietjen, C., Hahn, H.K.: Sketch-based image-independent editing of 3D tumor segmentations using variational interpolation. In: Eurographics Workshop on Visual Computing for Biology and Medicine, pp. 73–80. The Eurographics Association (2012)
4. Meyer, M., Desbrun, M., Schröder, P., Barr, A.H.: Discrete differential-geometry operators for triangulated 2-manifolds. Visualization and Mathematics 3(7), 34–57 (2002)
5. Boykov, Y., Funka-Lea, G.: Graph Cuts and Efficient N-D Image Segmentation. Int. J. of Comp. Vis. 70(2), 109–131 (2006)
6. Reuter, M., Biasotti, S., Giorgi, D., Patanč, G., Spagnuolo, M.: Discrete laplace-beltrami operators for shape analysis and segmentation. Computers & Graphics 33(3), 381–390 (2009)
7. Davis, T.A.: Algorithm 832: Umfpack v4. 3—an unsymmetric-pattern multifrontal method. ACM Transactions on Mathematical Software (TOMS) 30(2), 196–199 (2004)
8. Yushkevich, P.A., Piven, J., Cody, H., Ho, S., Gee, J.C., Gerig, G.: User-guided level set segmentation of anatomical structures with itk-snap. Insight Journal, Special Issue on ISC/NA-MIC/MICCAI Workshop on Open-Source Software (2005)